

Relocation of the 2006 M_w 6.1 Silakhour, Iran, Earthquake Sequence: Details of Fault Segmentation on the Main Recent Fault

by Abdolreza Ghods, Mehdi Rezapour, Eric Bergman,
Gholamreza Mortezaejad, and Morteza Talebian

Abstract The M_w 6.1 Silakhour earthquake occurred on 31 March 2006 in the Zagros region of Iran. It was preceded by two relatively large foreshocks of m_b 4.8 and 5.2 on 30 March and followed by an extensive aftershock sequence. The earthquake sequence occurred along the right-lateral strike-slip Main Recent Fault (MRF). To understand the spatial relationship between the mainshock and the high level of foreshock and aftershock activity, we have merged all seismic data recorded by Iranian seismic networks with data from the global catalogs and relocated the events using a multiple-event relocation method. We also conducted source studies of the mainshock and larger foreshocks and aftershocks, which confirm dominantly right-lateral strike-slip faulting for the mainshock, the two large foreshocks, and the largest aftershock. The relocated epicenters of the 2006 earthquake sequence lie close to the MRF and spread parallel to the MRF over a distance of ~ 55 km, much longer than the 15–20-km rupture length to be expected of a magnitude 6.1 strike-slip earthquake. The relocated epicenters reveals that the seismic sequence is divided into two parts, an eastern patch on the Borujerd–Dorud segment of the MRF that is directly associated with the rupture of the mainshock and a second patch, 20–25 km long, on the Nahavand–Borujerd segment of the MRF. The two patches are offset by ~ 5 km in the same sense as the MRF. The pattern of the western patch of seismicity strongly suggests a seismically active lineation that does not correspond closely to the mapped faults of the area. We take this as evidence of ongoing evolution of fault geometry on this section of the MRF. Coulomb stress calculations suggest that the seismicity on the Nahavand–Borujerd segment may be a separate earthquake sequence, triggered by static stress changes related to the mainshock rupture.

Introduction

The M_w 6.1 (Global Centroid Moment Tensor) Silakhour (named after the Silakhour Plain) earthquake occurred at 1:17 UTC on 31 March 2006 in Lorestan province in western Iran. It has been variously referred to as the Lorestan, Borujerd, Dorud, Chalan-Chulan, and Darbe Astaneh event. The U.S. Geological Survey (USGS) reported the epicenter at 33.50° N, 48.78° E, close to the Main Recent Fault (MRF, Fig. 1) between the cities of Borujerd and Dorud (Fig. 2).

The 2006 Silakhour event was preceded by two relatively large foreshocks of m_b 4.8 (at 16:17 UTC on 30 March) and m_b 5.2 (at 19:36 UTC on 30 March) and followed by two relatively large aftershocks of m_b 4.7 and 4.9 at 01:31 and 11:54 UTC, respectively, on 31 March. Many smaller aftershocks were recorded over a period of about a month after the mainshock. The significant foreshock activity and larger than usual aftershock cloud related to this earthquake of

moderate magnitude is a major reason for our interest to better understand the detailed pattern of seismicity and its relationship to the major fault structures in the area.

The Building and Housing Research Center (BHRC) reported that about 300 villages in the Silakhour plain were seriously affected by the earthquake; 68 people were killed, and about 2000 were injured (Mirzaie Alevijeh *et al.*, 2006). Given the relatively dense population of the affected area and the poor construction quality that is typical of the region, the human loss was far less than expected. This is largely due to the two large foreshocks, which alarmed many people, causing them to leave their homes.

The Global (formerly Harvard) Centroid Moment Tensor (CMT) solution (strike/dip/slip = 313/78/–174) indicates a mostly right-lateral strike-slip motion on a fault plane parallel to the MRF, dipping at 78° to the northeast.

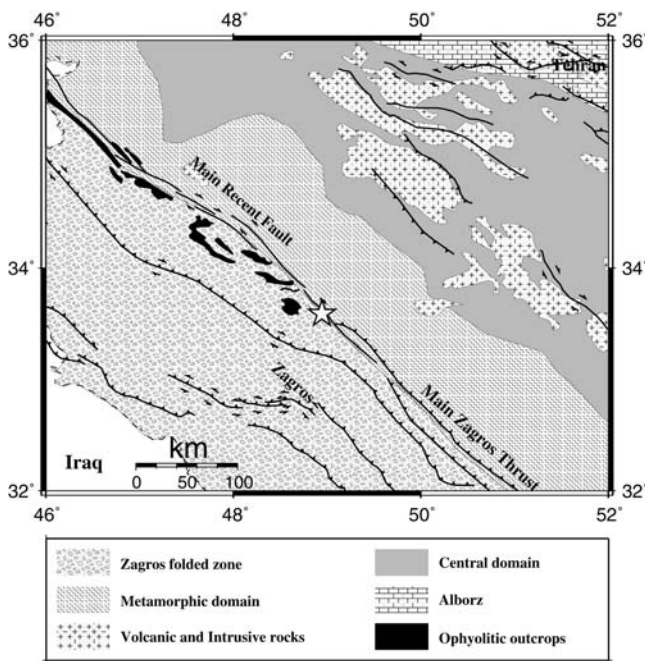


Figure 1. Major tectonostratigraphical units and fault systems of western Iran. Faults from Hessami *et al.* (2003). Geological provinces are modified from the structural map of the National Geoscience Database of Iran (NGDIR; see Data and Resources). The epicenter of the 2006 Silakhour mainshock, as calculated by this study, is shown by a white star. The solid lines show fault traces.

The USGS moment tensor solution was very similar but preferred a shallower dip angle (strike/dip/slip = 314/54/180). A body waveform inversion study by James Jackson (presented in Peyret *et al.*, 2008) estimates a similar mechanism with intermediate dip angle (strike/dip/slip = 318/63/174).

The centroid depth of the mainshock was estimated at 7 km by the USGS from their moment tensor study, and 6 km by Jackson's body waveform inversion. The Global CMT methodology does not provide good depth resolution for shallow events, but their centroid depth of 12 km is consistent with the shallow depths suggested by higher-resolution methods. Jackson estimated a source-time function of about 10-s total duration but consisting of two shorter pulses, one of about 4-s duration followed by one of 3-s duration.

Peyret *et al.* (2008) have published a slip model of the mainshock based mainly on Interferometric Synthetic Aperture Radar (InSAR) and geodetic data. Their slip model is consistent with the faulting geometry determined from seismic data (indeed, it was partially constrained by that data) and constrains the extent of rupture to ~15 km along strike and ~6 km down-dip, centered at ~5 km depth, on a fault plane that intersects the surface at the mapped surface trace of the MRF. We will discuss the comparison of these results with our own in the Relationship to the Main Recent Fault section. It should be noted that the InSAR data imply that the rupture was most likely to have occurred on the northeast side of the surface trace of the MRF, whereas all initial regional and teleseismic locations place the epicenter to the

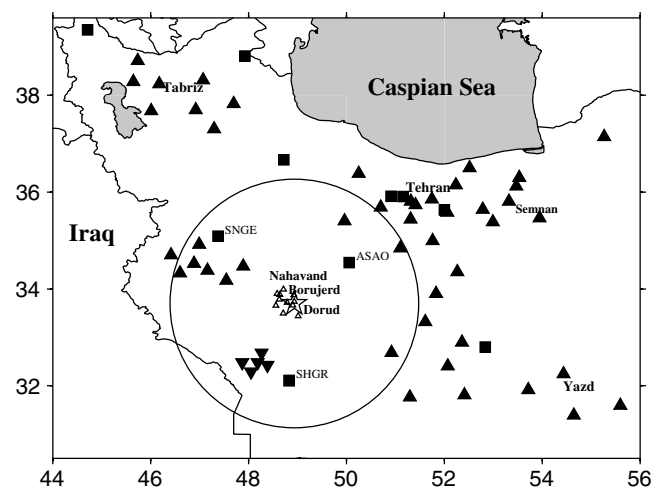


Figure 2. Seismic stations in the vicinity of the 2006 Silakhour sequence. The black triangles, squares, inverse triangles, and the small white triangles correspond to temporary stations belonging to the Iran Telemetered Seismograph Network (ITSN), Iranian National Seismograph Network (INSN), Karkheh dam networks, and temporary International Institute of Earthquake Engineering and Seismology (IIEES) network, respectively. The large star shows the epicenter of the Silakhour main event. A circle of radius 222 km (~2.0°) is shown to indicate the sampling of the seismic networks that was used to estimate the hypocentroid in the calibrated hypocentroidal decomposition (HDC) analysis.

south of the MRF. It is a specific goal of our study to resolve this discrepancy with a careful relocation exercise.

The 2006 Silakhour event produced local landslides and many surficial effects (MahdaviFar and Tajik, 2008) but did not produce significant surface rupture. Field investigations, carried out the day following the main event by the Geological Survey of Iran, identified a short zone of discontinuous fissuring with an overall trend of northwest–southeast near the village of Chalan-Chulan, a few meters southwest of the fault escarpment related to long-term motion on the MRF. The northwest-trending cracks exhibited a step to the left, consistent with right-lateral motion of the fault. These features were washed out by heavy rain two days after the earthquake, preventing further investigation of these or any other surficial features that might have provided evidence on the location and extent of rupture.

Our prime interest in this study is to unravel the details of the foreshock–mainshock–aftershock sequence and understand it in the context of the known geometric complexities of the MRF in the source region. Our approach to this problem is to relocate as many events as possible in the sequence by gathering all available phase arrival data from permanent seismic stations in Iran, as well as observing stations worldwide, and to use specialized location procedures to obtain location errors smaller than 5 km (in both relative and absolute terms). We have also used a small amount of data from a temporary deployment of seismometers to monitor aftershocks for calibration of the absolute locations of the larger earthquakes (Yamini-Fard, personal commun.,

2011), but we did not have access to the full data set from that deployment.

Using regional waveforms, we calculate moment tensors for the main event, the two foreshocks, and one aftershock event. Using waveform data from strong-motion stations, we calculate depths for the large events in the cluster. In addition, using crustal depth phases, we determine depths for a subset of the aftershock events. Finally we investigate the possibility that the seismicity on the Nahavand–Borujerd segment should be considered as a separate earthquake sequence that was triggered by static stress changes related to the mainshock rupture. This study offers the first aftershock study of this type done for the MRF and provides insights into the behavior of this complex fault system.

Seismotectonic Background

The MRF lies within the northwestern section of the Zagros Mountains of western Iran; it is the most seismically active fault system in this area. In this part of the Zagros, convergence between the Arabian and Eurasian plates is oblique to the trend of the orogenic belt (Jackson, 1992; De Mets *et al.*, 1994; Chu and Gordon, 1998). Talebian and Jackson (2002) suggest that the oblique convergence is accomplished by spatial separation of strike-slip and shortening components on separate parallel faults. The strike-slip component appears to be mainly along the MRF (Tchalenko and Braud, 1974).

The MRF changes trend along its length, from $\sim 330^\circ$ in the northwest, between Nahavand and Borujerd, to 300° in the central part and 315° in the Dorud–Borujerd basin, where it ends in several splay faults (Fig. 3). The Nahavand–Borujerd segment of the MRF (northwest of Borujerd) is referred to in this study as the Nahavand segment, while the Borujerd–Dorud segment of the MRF is referred to as the Dorud segment. Based on the geomorphology along the northwestern and southeastern segments of the MRF, as well as focal mechanism of earthquakes, Talebian and Jackson (2002) suggest that the overall slip vector is almost parallel to the central segment, implying a component of normal faulting along the Dorud segment of the MRF. In addition, there is a right-step in the strike-slip faulting on the northwest side of the Dorud–Borujerd basin that leads to local extension (pull-apart) and along-strike growth of the basin. Thus the northwest end of the basin, south of Borujerd, is an area of complex faulting with at least two trends, one parallel to the MRF with a mainly strike-slip mechanism and the other characterized by normal faults with oblique orientation that bound the basin in the northwest.

The largest historical earthquake in the area, a magnitude M_s 7.4 event, occurred near Dorud on 23 January 1909 (Ambraseys and Moinfar, 1973). The full length of rupture is at least 45 km but may be as great as 65 km, depending on the interpretation of less convincing evidence in the southeastern portion of the rupture zone, southeast of Darbe Astaneh (Ambraseys and Melville, 1982). The fault

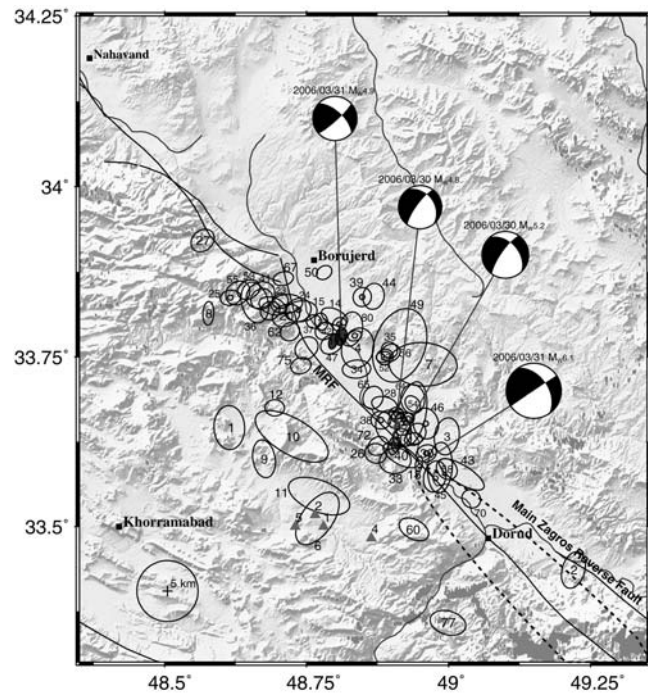


Figure 3. Relocation of 80 Silakhour events, from 1961 through September 2006, using the HDC multiple-event relocation method; 90% confidence ellipses for the relative locations of epicenters are shown to reveal the seismicity pattern. Event numbers correspond to Table 2. Event number 18 (shown in white) is the epicenter of the 31 March 2006 mainshock. The two largest foreshocks are shown in light gray; the two largest aftershocks are shown in dark gray. Events having a reliable depth determination (Table 2) are marked with small gray circles. Epicenter determinations for the mainshock from other agencies are shown by small triangles, numbered as in Table 4. Fault traces are shown in black. The Nahavand–Borujerd segment of the MRF (northwest of Borujerd) is referred to in this study as the Nahavand segment, while the segment of the MRF between Borujerd and Dorud is referred to as the Dorud segment. The dashed ellipse shows the approximate rupture extent of the 23 January 1909 M_s 7.4 event, from Ambraseys and Melville (1982). The focal mechanisms of the mainshock, the two foreshocks, and one aftershock from waveform modelling done in this study are also indicated. The location of important cities is shown by black squares. The circle in the lower left corner has a radius of 5 km for scale.

trace shown in Ambraseys and Melville (1982) is equivalent to what is now named the MRF, but they report that there was no field evidence for strike-slip rupture—only vertical displacements (north-east side down). The northwestern limit of rupture of this event, as reported by Ambraseys and Melville (1982), has been indicated on the MRF in Figure 3.

Data and Methodology

Global seismic networks can only locate a handful of the larger events of the Silakhour sequence, with a location error of a few tens of kilometers. Location accuracy is limited by the necessity to use a standard 1D Earth model

for global (and even most regional) catalogs. Variable network coverage for individual events interacts with the unmodeled 3D structure of the Earth in unpredictable but significant ways to produce location bias (e.g., [Bondar et al., 2004](#)). The trend of location bias is often broadly consistent over a given region, but the bias for specific events is unpredictable. Therefore, global network locations have little value for a detailed seismotectonic study of this kind. The location of epicenters reported by the USGS for the study region suggests that most seismicity in this area occurs to the southwest of the MRF and the number of events that have been located is too small to permit detailed seismotectonic analysis.

Modern Iranian network seismology begins in the mid-1990s, with the start of deployment of the Iran Telemetered Seismograph Network (ITSN), a series of small regional subnetworks by the Institute of Geophysics of Tehran University. These short-period stations were joined in the early 2000s by the Iranian National Seismograph Network (INSN), a network of about a dozen broadband satellite-telemetered stations operated by the International Institute of Earthquake Engineering and Seismology (IIEES); other organizations have also added seismic stations for specialized monitoring projects. See [Data and Resources](#) section for details. A review of the operation of the Tehran subnetwork of the ITSN has been provided by [Ghods and Sobouti \(2005\)](#).

For this study, all available waveforms of the Silakhour earthquake sequence from Iranian stations (29 stations in all) were compiled from the organizations listed herein, and P and S arrival times were picked using SEISAN software ([Havskov and Otemoller, 1999](#)) by one of us. Sampling rates are 100 samples per second (sps) for INSN waveforms and 50 sps for ITSN waveforms. Picking errors are always less than 0.1 s for readings given full weight.

Figure 2 shows the distribution of permanent seismic stations in the vicinity of the Silakhour seismic sequence. The stations belong to the ITSN, INSN, and Karkheh dam networks. The distribution of a temporary network deployed by IIEES is also shown in Figure 2. In addition, the BHRC network of digital accelerometers recorded the foreshocks, mainshock, and several of the larger aftershocks at short epicentral distances. The BHRC data (200 sps) are used to independently confirm the accuracy of the location of the main event and estimate focal depth for a subset of the seismic sequence.

For stations outside of Iran, we relied almost entirely on picks reported in standard bulletins, such as the International Seismological Centre (ISC), U.S. Geological Survey Preliminary Determination of Epicenters (PDE), and European Mediterranean Seismological Center (EMSC) bulletins. Arrival time uncertainties are not reported by these bulletins, but we estimate reading errors (for each station–phase pair) empirically during the hypocentroidal decomposition relocation process described in the [Multiple-Event Relocation](#) section.

This study is arguably the first time that Iranian permanent seismic networks were able to monitor an extended seismic sequence associated with a large earthquake at short epicentral distances and with relatively good azimuthal coverage.

Single-Event Locations

The events of the Silakhour sequence have been located first with a standard single-event approach, the program HYPOCENTRE ([Lienert and Havskov, 1995](#)), which is ported into the SEISAN software package. We used a modified version of a 1D velocity model ([Doloei and Roberts, 2003](#); [Kaviani, 2004](#); [Tatar, 2001](#)) that is routinely used for locating local and regional events in Iran (Table 1).

A total of 189 events from 1 January to 30 June 2006 were relocated, and 140 of these events were located with 10 or more stations. For six stations, mostly belonging to the Kharkeh dam network (Fig. 2), timing problems limited us to the use of relative phase times (S_g – P_g) in the location procedure. Although epicenters are well constrained by this analysis, the data set was found to have little ability to resolve focal depth because there are no close stations. The closest station that is well represented in the data set is ~140 km away.

The single-event locations were used as starting locations for the multiple-event relocation analysis.

Multiple-Event Relocation

To further explore the complex pattern of seismicity within the Silakhour sequence, we applied a method for multiple-event relocation that has been developed especially to carry out studies of location calibration (i.e., studies in which location bias from unknown Earth structures is minimized). The method is based on the hypocentroidal decomposition (HDC) method of multiple-event relocation described by [Jordan and Sverdrup \(1981\)](#). The key feature of the algorithm is the decomposition, through orthogonal projection operators, of the multiple-event relocation problem into two independent inverse problems:

Table 1
Crustal Velocity Model*

Layer	P Velocity (km/s)	Depth to Top of Layer (km)
1	5.4	0
2	6.0	6.0
3	6.3	14
4	6.5	18
5	8.05	51
6	8.1	80

*Modified standard crustal model ([Doloei and Roberts, 2003](#); [Kaviani, 2004](#); [Tatar, 2001](#)) used in single-event earthquake location in Iran. Moho is at 51 km instead of 48 km. A V_P/V_S ratio of 1.73 is used to derive the S velocities.

1. Estimation of a set of cluster vectors for each event that describe the location and origin time of each event with respect to the hypocentroid, the geometrical mean of the current locations.
2. With the relative locations fixed by the cluster vectors estimated in step 1, inversion for an updated location and origin time for the hypocentroid in geographic coordinates, using whatever subset of arrival time data is deemed most suitable for the problem. (This inversion is very equivalent to single-event location.)

Note that the data sets used in the two steps are not required to be identical. In fact, they may be completely disjointed. When the cluster vectors are added to the hypocentroid, the events take on absolute coordinates. As a general rule, we wish to use all available data for estimating the cluster vectors because this inversion is based on travel-time differences and the bias related to the unmodeled 3D Earth structure is therefore minimized. For the hypocentroid, on the other hand, we seek to use the portion of the data set that is considered least susceptible to the effects of the unmodeled 3D Earth structure to obtain a stable location. Typically, we restrict the estimation of the hypocentroid to direct-arriving phases (i.e., Pg and Sg phases), and it is desirable to restrict even those phases to the nearest distance range that can still provide adequate azimuthal coverage.

Using the redundancy of multiple samples of the same station-phase observed from different earthquakes within a restricted source region, we estimate empirical reading errors from the spread of residuals for each station-phase pair. The estimate is made with a robust estimator of spread (Croux and Rousseeuw, 1992) that works well for small sample sizes and imposes no assumption about the parent distribution. Reading error in this sense includes traditional picking error as well as other sources of spread in the observed arrival times (across events that may span many years), such as the differing philosophy or skill at phase picking of different analysts at an observatory, changes in instrumentation at an observatory, and timing errors. It also absorbs variability in travel times caused by slight differences in the ray paths from different events in the cluster to the observing station. This approach automatically accounts for changes in instrumentation and observatory practice over long time periods and allows us to combine earthquakes from early in the twentieth century with modern earthquakes for relocation.

Empirically-determined reading errors range in magnitude from a few tenths of seconds to several seconds. We enforce a minimum reading error of 0.15 s, based on observations from very-high-quality readings of impulsive sources, to prevent numerical problems. Empirical reading errors are used to weight the data and also to identify outliers in a statistically consistent manner. The process results in a data set for inversion that comes much closer than usual to satisfying the assumption of a Gaussian distribution and allows us to make reliable estimates of uncertainty in the

resulting locations. Recent applications of the method may be found in Walker *et al.* (2005), Biggs *et al.* (2006), Parsons *et al.* (2006), Tatar *et al.* (2007), and Bondar *et al.* (2008), in which the HDC algorithm is tested against a cluster of events (nuclear tests) with known hypocentral parameters.

For the study of the Silakhour sequence, we assembled a cluster of 80 events, beginning with a moderate-sized event on 28 October 1961 and ending on 28 September 2006. Sixty-five of the events in the cluster are associated with the 2006 Silakhour sequence, including the two large foreshocks. The data set of arrival times for these events was compiled from the standard global bulletins [PDE, ISC, and International Seismological Summary (ISS); see [Data and Resources](#)] and the special data set of repicked waveforms from Iranian seismic network stations described previously in this paper. We also utilized a set of arrival times for Pg and Sg , for the events in common to both data sets, from the temporary seismic network deployed by scientists from IIEES. We calculated empirical reading errors of the repicked Iranian waveform data and the temporary network readings in the same manner as for bulletin readings. The selection of events to be retained in the relocation analysis was determined by the quality of the solutions that could be obtained with the available data. That is, we discarded events with small numbers of arrivals, inconsistent readings, or with poor azimuthal coverage that led to confidence ellipses for the epicenter that were too large (roughly, with the largest semi-major axis greater than ~ 7 km) to be useful for seismotectonic interpretation. The smallest events in the cluster have magnitudes near 2.0.

The HDC method is not well suited to resolving focal depths unless the data set includes an exceptional number of readings from very close stations or teleseismic depth phases. This is not the case for the Silakhour cluster, so all focal depths are fixed at 7 km, based on other studies considered reliable for the depth of the mainshock. The USGS broadband depth analysis for the mainshock gives a centroid depth of 7 km. A similar depth (6 km) is obtained by analysis of teleseismic body waves (James Jackson, published in Peyret *et al.*, 2008), and the slip distribution model of Peyret *et al.* (2008) places the centroid of rupture at ~ 5 km depth. Finally, our own analysis of the BHRC accelerometer data (described subsequently in the [Depth Determination](#) section of this paper) confirms a shallow depth (6 km) for the mainshock. A few events in the cluster have teleseismic depth phase readings, and these were found to be consistent with depths in the range of 5–15 km. Experiments show that errors of assumed depth of less than ~ 15 km have a negligible effect on epicenter accuracy in the HDC analysis, and we are confident that the error in assumed depth for most events in the cluster is less than this.

To constrain the cluster vectors (relative locations), we used all available phase data (except the readings from temporary stations) at all epicentral distances; however, because HDC (like all multiple-event relocation methods) uses travel-time differences to constrain relative locations,

only station–phase pairs that are observed for two or more events in the cluster contribute to the estimate of the cluster vectors. After the various filtering operations to obtain a high-quality data set, 3383 readings were used to estimate the cluster vectors (240 free parameters). The uncertainties of relative location, described by the length of the largest semi-axis of the 90%-confidence ellipse for the cluster vector, range from 1.0 to 6.7 km, with most being less than 3 km.

The cluster vectors describe only relative locations of the earthquakes. Assignment of absolute coordinates for the cluster events depends on the solution for the hypocentroid of the cluster, a virtual event that is defined as the geometric center of the cluster. To use regional and teleseismic arrivals for this purpose would introduce bias because of the unknown effects of the 3D Earth structure. Short ray paths ensure that any errors in theoretical travel times will not accumulate to significant levels. If the confidence limits on the hypocentroid's location are small enough (typically less than 5 km), we refer to the resulting locations as being calibrated, and we assert that the hypocentroid located in this manner is subject to minimal bias from unknown Earth structure, in the same way that minimally biased locations can be generated by locating individual earthquakes with data sets of arrival times from well-distributed stations restricted to short epicentral distances (Bondar *et al.*, 2004). This method of calibrating the absolute locations of clusters of earthquakes is very similar to the reciprocal cluster analysis (RCA) method described in Bondar *et al.* (2008) and has been thoroughly tested against the RCA method.

We estimated the location of the hypocentroid of the Silakhour earthquake cluster using arrival times from the temporary seismograph network deployed by IIEES (Yamini-Fard, personal commun., 2011) that recorded many of the events in our HDC cluster. The locations of the stations are shown in Figure 2. We used 305 P_g and S_g readings, all at distances of less than 0.5° for the calibration, to estimate the location of the hypocentroid with a formal uncertainty of 1.0 km. The true uncertainty is undoubtedly larger, mainly because of uncertainty about the velocity structure and fixed depths, but is highly unlikely to be greater than 2–3 km.

The results of the HDC analysis are shown in Figures 3 and 4 and listed in Table 2. In Figure 3, we have shown the confidence ellipses for relative locations (i.e., the cluster vectors) in order to better reveal the details of the seismicity pattern. When the uncertainty of the hypocentroid is added to the uncertainties of the individual cluster vectors (through conversion of both ellipses to matrix form, addition, and conversion back to elliptical form), the final estimate of location error for any individual event in the Silakhour sequence ranges from 2.1 to 7.0 km, with most being less than 4 km. Confidence ellipses in Table 2 are for absolute location, at the 90%-confidence level. The confidence ellipse (for absolute location) for the 31 March 2006 mainshock has a semi-major axis of 2.2 km oriented at 178° . In Figure 3, the confidence ellipse (cluster vector only) is somewhat smaller and slightly rotated.

Confirming the Location of the Mainshock

We use a completely independent data set to confirm the location of the 2006 Silakhour mainshock epicenter determined in the calibrated HDC analysis. The Silakhour mainshock was recorded by 26 accelerometer stations operated by BHRC. Figure 5 shows the locations of the nearby BHRC stations and the vertical component of the recorded accelerograms. Figure 5 explicitly shows that the main event has been recorded with fairly good azimuthal coverage and short epicentral ranges, and thus good location accuracy can be expected. It is unfortunate, however, that a station in Borujerd failed to operate during the mainshock. It is also unfortunate that absolute arrival times cannot be used for the location, because these instruments did not have calibrated timing systems. Our location is therefore done with differential times calculated from our picks of P_g and S_g arrivals, which significantly reduces location precision because the derivative of S_g – P_g times changes slowly with epicentral distance. One seismic station (ASAO) is included to provide a time base. The accuracy of the relative phase arrival readings is judged to be within 0.2–0.4 s. The epicenter of the mainshock as calculated from the accelerometer data set differs by ~ 8 km (to the northeast) from the location calculated with the HDC analysis (Fig. 5). We consider this location to be in reasonable agreement with the HDC location, given the uncertainties in using S_g – P_g readings for location.

Depth Determination

For the mainshock and its two large foreshock and two large aftershocks, there is one accelerometer station with epicentral distance less than 10 km. The station at Chalan-Chulan (Chal in Fig. 5) is very close to the epicenters of the mainshock and foreshocks, and the Boroujerd station is very close to the aftershocks. We used S_g – P_g phase readings to estimate the depths for these events, given the calibrated locations. A depth of 6 km is calculated for the mainshock, which is in full agreement with the depth determined by body waveform inversion (Peyret *et al.*, 2008). The depth of both large foreshocks is determined to be 7 km. Depths of 7 and 15 km are calculated for the first (m_b 4.7 at 01:31 UTC on 31 March) and second large aftershocks (m_b 4.9 at 11:54 UTC on March 31), respectively. The depths inferred from accelerometer data confirm our assumption of a shallow depth for the HDC analysis, and they are consistent with the depth range determined by Peyret *et al.* (2008) for the main rupture.

For a subset of 18 events (larger aftershocks, including the five events described in the preceding paragraph), we also estimated focal depths using differential regional sP_g – P_g phase readings. The method is fully described by Ma and Atkinson (2006). For 17 events, station ASAO (Fig. 2) is used to read the sP_g – P_g differential phase. For the second large aftershock, station SHGR (Fig. 2) is used. The estimated depths, ranging from 7 to 14 km, are listed in Table 2. For the events in common, there is good agreement in

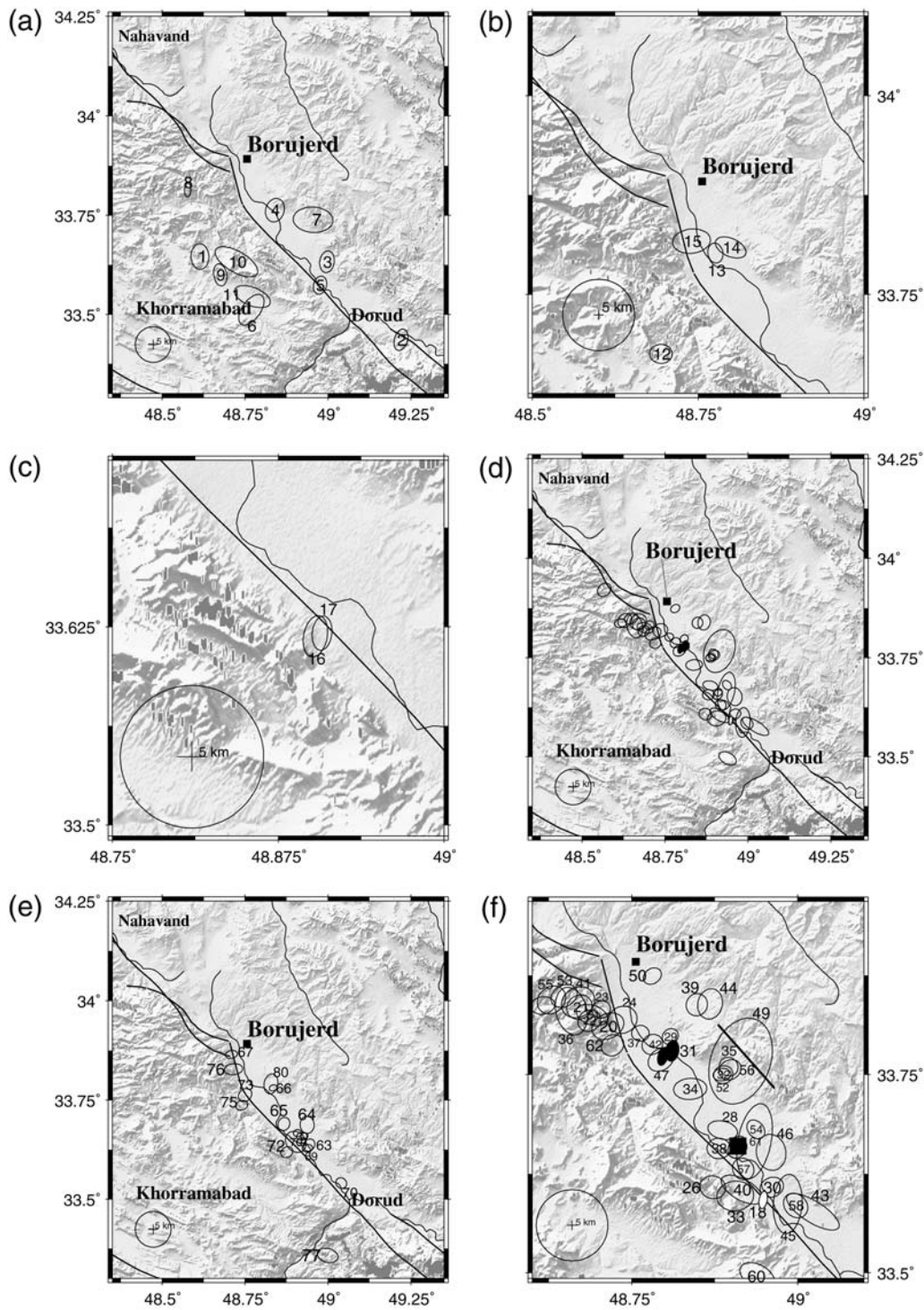


Figure 4. The 80 events in the HDC analysis (Fig. 3) are shown in five chronological stages and a summary view of the immediate rupture area: (a) events from 1961 through 2001; (b) events in May and June of 2005; (c) the two foreshocks, (d) the mainshock on 31 March and aftershocks for the first eight days (through 8 April 2006); (e) aftershocks from 9 April to the end of the cluster on 28 September; and (f) a closer view of the mainshock and eight-day aftershocks (c.f., Fig. 4d), with a large solid black box indicating the location of the village Chalan-Chulan, and a solid black line indicating the approximate extent of the gap in seismicity between the Nahavand and Dorud patches. The location of important cities is shown by small black squares.

estimated depths between this method and the determination based on BHRC data. The depths of the events in the Dorud segment increase with distance from the MRF in agreement

with the dip of the fault plane to the northeast. The epicenters of the events for which a focal depth was determined are marked on Figure 3 with a gray circle.

Table 2
List of Relocated Epicenters*

Event Number	Date (yyyy/mm/dd)	Time (UTC; hh:mm:ss.ss)	Latitude	Longitude	Depth (km)	m_b/M_L	M_s	M_w	AZI [†]	L1 [†]	AZ2 [†]	L2 [†]	Area (km ²) [†]	Depth (km) [‡]
1	1961/10/28	10:46:39.20	33.646	48.6095	7	0	0	0	86	31	176	41	40	
2	1975/09/01	23:15:53.35	33.436	49.2155	7	4.9	0	0	284	26	14	36	30	
3	1982/09/01	07:19:05.85	33.633	48.9925	7	4.8	3.5	0	277	28	7	36	31	
4	1983/12/26	03:48:21.58	33.763	48.8355	7	4.5	0	0	283	32	13	38	38	
5	1985/11/23	19:31:56.23	33.574	48.9715	7	4.7	0	0	281	26	11	32	26	
6	1989/10/10	14:57:40.66	33.512	48.7645	7	4.6	0	0	305	32	35	52	53	
7	1994/09/02	23:29:38.27	33.739	48.9505	7	4.3	0	0	4	40	94	59	74	
8	1999/08/01	19:22:50.77	33.814	48.5725	7	4.6	0	0	88	21	178	27	17	
9	2001/10/16	23:42:14.59	33.6	48.6705	7	3.9	0	0	78	26	168	37	30	
10	2001/10/17	08:21:04.45	33.633	48.7195	7	0	0	0	31	34	121	70	75	
11	2001/10/18	01:52:10.75	33.545	48.7675	7	0	0	0	22	31	112	56	55	
12	2005/05/02	22:31:23.64	33.675	48.6895	7	3.1	0	0	19	23	109	25	18	
13	2005/05/03	07:21:10.25	33.802	48.7715	7	4.9	0	4.9	69	21	159	24	16	
14	2005/05/03	07:24:26.46	33.809	48.7945	7	0	0	0	27	22	117	30	21	
15	2005/06/05	10:19:18.23	33.817	48.7355	7	3.5	0	0	357	25	87	32	26	
16	2006/03/30	16:17:05.94	33.619	48.8985	7	4.8	0	0	271	20	1	24	15	6 ⁺
17	2006/03/30	19:36:16.95	33.621	48.9035	7	5.2	0	5.1	82	20	172	22	14	7 ⁺
18	2006/03/31	01:17:01.07	33.592	48.9435	7	5.7	6	6.1	88	19	178	22	14	6 ⁺
19	2006/03/31	01:31:23.24	33.773	48.7925	7	4.7	0	0	274	20	4	23	14	7 ⁺
20	2006/03/31	02:01:14.17	33.811	48.7095	7	2.5	0	0	338	26	68	29	24	
21	2006/03/31	02:08:57.09	33.835	48.6665	7	2.5	0	0	339	25	69	26	20	
22	2006/03/31	02:12:26.88	33.818	48.6815	7	2.4	0	0	337	24	67	24	18	
23	2006/03/31	02:42:34.12	33.832	48.6995	7	2.3	0	0	33	22	123	23	16	
24	2006/03/31	02:48:28.32	33.819	48.7315	7	3.3	0	0	344	27	74	28	23	9
25	2006/03/31	02:58:28.05	33.837	48.6115	7	2.7	0	0	1	22	91	25	18	11.5
26	2006/03/31	05:03:07.99	33.608	48.8675	7	2.2	0	0	28	24	118	26	20	
27	2006/03/31	05:43:04.03	33.921	48.5625	7	2.5	0	0	318	25	48	27	22	
28	2006/03/31	06:30:00.34	33.68	48.8825	7	2.2	0	0	18	22	108	28	20	
29	2006/03/31	09:23:34.70	33.798	48.8035	7	2.6	0	0	53	22	143	22	15	9
30	2006/03/31	09:40:25.38	33.608	48.9565	7	2.4	0	0	353	23	83	25	18	12.5
31	2006/03/31	11:54:01.98	33.78	48.8065	7	4.9	4.3	5.1	90	21	180	24	16	14 ⁺
32	2006/03/31	15:30:08.84	33.75	48.8835	7	2.7	0	0	27	22	117	23	16	
33	2006/03/31	16:06:03.60	33.597	48.9015	7	2	0	0	359	28	89	32	28	
34	2006/03/31	17:02:18.26	33.732	48.8335	7	2	0	0	0	24	90	30	22	
35	2006/03/31	20:04:14.03	33.76	48.8915	7	2.2	0	0	47	22	137	24	16	
36	2006/04/01	01:56:46.30	33.83	48.6545	7	2.3	0	0	74	28	164	39	34	
37	2006/04/01	05:23:02.58	33.802	48.7585	7	2.4	0	0	32	21	122	23	15	
38	2006/04/01	06:12:37.98	33.657	48.8765	7	2.8	0	0	21	23	111	25	18	9

(continued)

Table 2 (Continued)

Event Number	Date (yyyy/mm/dd)	Time (UTC; hh:mm:ss.ss)	Latitude	Longitude	Depth (km)	m_b/M_L	M_s	M_w	$AZ1^\dagger$	$L1^\dagger$	$AZ2^\dagger$	$L2^\dagger$	Area (km 2) ‡	Depth (km) ‡
39	2006/04/01	08:31:05.77	33.838	48.8435	7	4.1	0	0	66	24	156	24	18	12
40	2006/04/01	09:13:37.39	33.605	48.9115	7	2.5	0	0	31	23	121	37	27	
41	2006/04/01	09:35:55.91	33.841	48.6645	7	2.2	0	0	330	28	60	30	27	
42	2006/04/01	10:27:23.36	33.788	48.7765	7	2.3	0	0	30	23	120	24	17	
43	2006/04/01	11:58:57.69	33.577	49.0185	7	2.4	0	0	32	24	122	46	34	
44	2006/04/01	12:08:33.45	33.839	48.8635	7	4.2	0	0	274	25	4	28	23	
45	2006/04/01	13:40:34.71	33.587	48.9805	7	2.5	0	0	273	27	3	46	39	
46	2006/04/02	01:59:03.85	33.652	48.9555	7	4.2	0	0	74	27	164	32	27	10
47	2006/04/02	14:36:40.91	33.769	48.7895	7	2.7	0	0	325	24	55	26	20	9
48	2006/04/02	19:25:59.34	33.663	48.9065	7	3.8	0	0	61	21	151	22	14	8.5
49	2006/04/02	21:44:43.60	33.767	48.9095	7	2.1	0	0	289	46	19	65	93	
50	2006/04/03	02:58:59.16	33.874	48.7765	7	2.9	0	0	338	22	68	23	15	
51	2006/04/03	06:38:44.28	33.825	48.6855	7	2.6	0	0	24	23	114	30	21	
52	2006/04/03	23:09:12.58	33.75	48.8815	7	2.2	0	0	11	21	101	22	15	
53	2006/04/04	01:26:30.33	33.849	48.6435	7	2.5	0	0	336	24	66	26	20	
54	2006/04/04	05:56:46.29	33.681	48.9325	7	3.1	0	0	49	21	139	24	16	
55	2006/04/04	21:19:24.30	33.844	48.6245	7	2.3	0	0	315	26	45	28	23	
56	2006/04/06	00:45:25.67	33.756	48.8935	7	2.3	0	0	341	23	71	24	18	
57	2006/04/06	11:18:10.21	33.631	48.9135	7	2.5	0	0	49	23	139	25	18	
58	2006/04/06	15:28:35.88	33.585	48.9925	7	2.4	0	0	48	24	138	27	20	
59	2006/04/07	04:42:30.65	33.657	48.9045	7	2.3	0	0	307	23	37	23	17	
60	2006/04/07	15:06:17.71	33.496	48.9345	7	2.4	0	0	30	24	120	32	25	
61	2006/04/08	00:29:25.83	33.666	48.9305	7	2.6	0	0	281	30	11	57	53	
62	2006/04/08	09:41:16.41	33.787	48.7165	7	3	0	0	349	24	79	24	18	
63	2006/04/09	21:57:05.53	33.637	48.9385	7	2.4	0	0	294	24	24	26	19	
64	2006/04/12	11:47:39.59	33.688	48.9325	7	4.6	0	0	80	27	170	31	26	
65	2006/04/14	00:18:36.19	33.69	48.8625	7	2	0	0	278	25	8	26	21	
66	2006/04/14	08:42:18.49	33.781	48.8305	7	2.7	0	0	6	21	96	22	14	11
67	2006/04/19	18:56:36.34	33.865	48.7045	7	2.3	0	0	356	22	86	25	17	
68	2006/04/19	23:13:40.35	33.659	48.9245	7	4.4	0	0	43	21	133	21	14	9
69	2006/04/21	08:54:21.94	33.629	48.9335	7	2.6	0	0	6	21	96	24	16	7
70	2006/04/23	02:03:29.42	33.541	49.0355	7	2.6	0	0	45	23	135	25	18	
71	2006/04/24	00:28:05.08	33.667	48.9035	7	3.2	0	0	27	21	117	22	14	9
72	2006/04/27	13:08:03.94	33.619	48.8715	7	2.5	0	0	330	24	60	25	19	
73	2006/04/28	14:00:04.93	33.763	48.7455	7	2.3	0	0	319	26	49	27	22	
74	2006/04/29	16:39:13.53	33.645	48.9145	7	1.9	0	0	24	22	114	22	15	
75	2006/04/29	18:45:45.23	33.737	48.7355	7	2.4	0	0	354	23	84	25	18	
76	2006/04/29	21:31:32.90	33.828	48.7105	7	2.1	0	0	357	24	87	32	24	
77	2006/04/29	23:55:26.71	33.358	48.9945	7	2.1	0	0	19	27	109	35	30	

(continued)

Table 2 (Continued)

Event Number	Date (yyyy/mm/dd)	Time (UTC; hh:mm:ss.ss)	Latitude	Longitude	Depth (km)	m_b/M_L	M_s	M_w	AZ1 [†]	L1 [†]	AZ2 [‡]	L2 [‡]	Area (km ²) [†]	Depth (km) [‡]
78	2006/04/30	18:00:17.28	33.659	48.9165	7	2.8	0	0	3	22	93	24	16	9
79	2006/06/17	15:36:36.99	33.645	48.8985	7	4.4	0	0	48	32	138	37	37	
80	2006/09/28	10:11:12.85	33.791	48.8235	7	0	0	0	277	27	7	34	28	

*Epicenters determined using the HDC method, calibrated by locating the hypocentroid using only local distance data. Magnitudes for larger events are from the USGS when available. For smaller events, we calculated local magnitude (M_L) using the relationship of Hutton and Boore (1987).

[†]The 90% confidence ellipses for absolute location (summing uncertainties the cluster vectors and the hypocentroid) are described in columns 10–14: AZ1 and AZ2 are azimuths of ellipse semiaxes, and L1 and L2 are the corresponding semiaxis lengths, in km and scaled by a factor of 10. The Area column gives the area of the confidence ellipse.

[‡]The last column reports the depth of the events estimated by this study; the events for which the depth is estimated only by an *S-P* phase reading of BHRC stations are marked with a single “+” symbol; the events for which the depth is estimated by both *S-P* phase reading of BHRC stations and secondary depth phases are marked with two “+” symbols; and the depth of events without any “+” is estimated using only the depth phases.

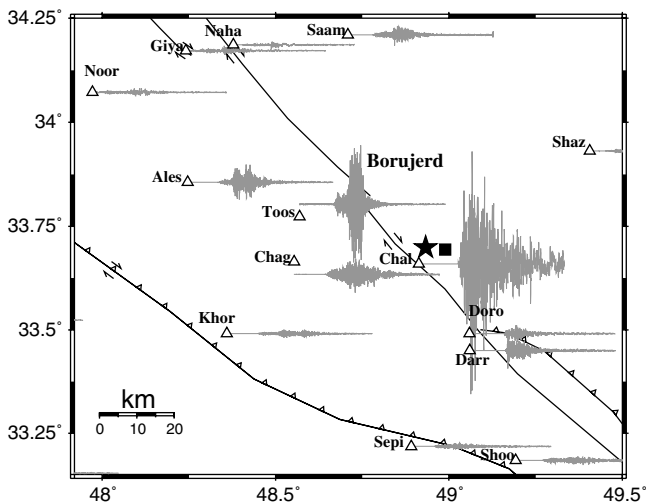


Figure 5. Waveforms of vertical BHERC accelerometric stations recorded the Silakhour mainshock. Only the waveforms of nearby BHERC stations that recorded the main event are shown in the map. A maximum record length of 60 s is shown, and the waveforms are drawn using equal scale for time and acceleration amplitude. Maximum and minimum acceleration amplitudes for Chal station are 4.51 and -5.23 m/s^2 , respectively. The epicenter, as located by HDC and single-event location based on BHERC data, is shown by a black star and rectangle, respectively. The location of accelerometer stations are shown by open triangles.

Point-Source Moment Tensor

Using waveforms of regional IIEES broadband stations and the method described by Dahm *et al.* (1999), we have performed waveform modeling to derive moment tensors for the main event, two foreshocks, and one aftershock. We inverted amplitude spectra (20–50-s period) while holding the depths fixed according to the depth determinations discussed previously in this paper. Figure 6 shows the details of the best-fitting amplitude spectra moment tensor solution for the main event. One-dimensional Green's functions are calculated using the reflectivity method (Muller, 1985) and the crustal velocity model listed in Table 1. The impact of unknown structural complexities could be significant at the periods used here (Dahm *et al.*, 2007). Good azimuthal distribution of stations should minimize bias from this cause.

The source parameters from the moment tensor analysis are listed in Table 3. We also performed the moment tensor inversion by fitting seismograms in the time domain and found similar results. The focal mechanisms of the best-fitting moment tensor solutions are plotted in Figure 3. The focal mechanisms of all four events are similar and are consistent with right-lateral slip on a northwest-trending fault plane that is dipping to the northeast. The source parameters for the main event are in good agreement with those reported by the USGS, Global CMT project, and Peyret *et al.* (2008), although our solution has a smaller dip angle of $\sim 45^\circ$. The aftershock has a steeper dip than the mainshock and foreshocks, implying that the Nahavand segment of MRF may be steeper than the Dorud segment.

Seismicity

The pattern of HDC relocated epicenters in Figure 3 can be characterized as a cloud of aftershocks that spreads to the northwest of the mainshock. This implies a unidirectional sense of rupturing for the main event, a topic to which we will return. The aftershock pattern includes both the Borujerd–Dorud and Nahavand–Borujerd segments of the MRF. The HDC analysis shows a separation of seismic activity into two distinct patches, with the western one being offset to the north by several kilometers. There is a gap of ~ 10 km length between them, except for a knot of intense activity near 33.75° N, 48.90° E, on the north edge of the Silakhour basin. The eastern patch, ~ 15 km in length, includes the 2006 mainshock (event 18) and represents the aftershocks directly related to its rupture zone. The role of the western patch is less clear. To gain a better understanding of the seismicity pattern determined in the HDC analysis, we subdivide the cluster according to specific time periods (Fig. 4), again showing the confidence ellipses for relative locations.

It is important to recall that we expect the confidence ellipses shown in Figures 3 and 4 to contain the true location only 90% of the time. In other words, approximately seven or eight of the events in the cluster are expected to have true (relative) locations outside their ellipses. This may account for some outlier events that do not fit the pattern established by the rest of the cluster.

Early Seismicity (1961–2001)

The distribution of earthquakes between 1961–2001 is shown in Figure 4a. It reveals a zone of seismicity offset ~ 10 – 15 km southwest from the MRF, which includes a moderate event in 1961 and a sequence of three small events (events 9–11; Table 2) on 16–18 October 2001. Several of the other events, with m_b between 4.3 and 4.7 (events 3, 4, 5, and 7) are found in the zone that was active again in 2006. There is no further seismicity (none that are well-recorded enough to be included in the cluster) until 2005.

The 2005 Earthquake Sequence

In May and early June 2005, a sequence of four events (events 12–15) occurred, including the m_b 4.9 Borujerd event (event 13) on 3 May (Fig. 4b). The first event of this series, however, was located to the south and is associated with the zone of seismicity shown in Figure 4a. The other three are associated with the right-step between the Dorud and Nahavand segments of the MRF at the western edge of the Dorud basin. Peyret *et al.* (2008) attempted to study the rupture of the 3 May 2005 event with InSAR data but failed to find a definitive signal. They assumed the IIEES location for this event, a few kilometers east–southeast from Borujerd, but our calibrated HDC analysis (Table 2, Fig. 4b) shows the event to be located southwest of this location, close to the edge of interferogram coverage. This may help explain the absence of a clear InSAR signal for the event.

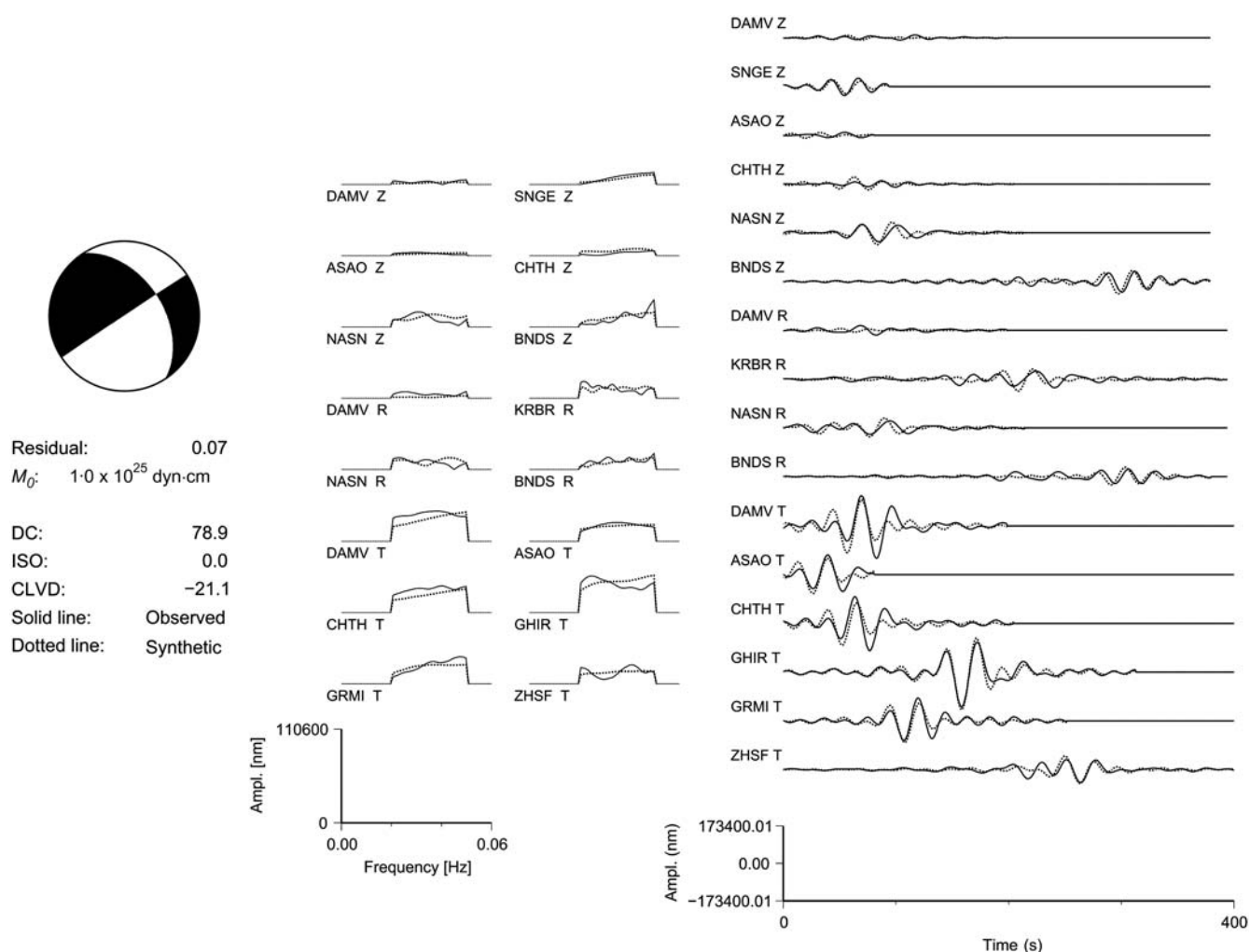


Figure 6. Minimum misfit solution for the 31 March 2006 Silakhour main event and comparison of observed and predicted amplitude spectrum from the best-fitted amplitude spectrum inversion (middle panel). The pass-band used in the inversion is 20–50 s. The vertical and horizontal axes show amplitude and frequency, respectively. The panel on the right compares the observed and predicted time series from the best-fitted amplitude spectrum inversion. The vertical and horizontal axes show amplitude in nm and time in seconds, respectively. The depth is fixed at 6 km. Detailed source parameters of the event are listed in Table 3.

Foreshocks

The two large (m_b 4.8 and 5.2) foreshocks of the 2006 Silakhour sequence (events 16 and 17 in Table 2) are shown in Figure 4c. Their locations are very tightly constrained and

are effectively identical. They are located very close to (but slightly southwest of) the surface trace of the MRF, in the middle of the aftershock zone that corresponds to the rupture zone of the 2006 Silakhour mainshock, 4–5 km northwest of the epicenter of the mainshock itself.

Table 3

Source Parameters for the Silakhour, Two Foreshocks, and One Aftershock*

Event	Strike (°)	Dip (°)	Rake (°)	Moment (dyn-cm)	Double Couple (%)
060330.1617	324.3	36.6	-157.7	9.6×10^{22}	87.75
060330.1936	318.7	45.5	-160.5	5.0×10^{23}	92.11
060331.0131	326.8	47.4	-178.9	1.0×10^{25}	78.91
060331.1154	312.9	63.4	170.1	3.4×10^{23}	92.98

*Source parameters were determined by moment tensor inversion by fitting the amplitude spectrum. The focal mechanisms are plotted in Figure 3.

Mainshock and Early Aftershocks

The 2006 mainshock at 01:17 hrs on March 31 (event 18) and the first eight days of aftershocks are shown in Figure 4d,f. The seismicity clearly divides into three main groups:

1. Events directly associated with the rupture of the mainshock on the Dorud segment of the MRF. These epicenters define a rupture zone of 10–15 km along strike, and perhaps 8–10 km across strike, in good agreement with other estimates of fault dimensions for this

event. Focal mechanism data show the fault to be dipping $\sim 60^\circ$ to the northeast, so the mainshock epicenter would be near the upper edge of the fault zone and toward the southeastern end of it. The pattern of epicenters is mainly confined to the Dorud basin but some events, including that of the mainshock, are located slightly southwest of the MRF surface trace. This is discussed in the [Relationship to the Main Recent Fault](#) section.

2. Events associated with a 20-km long segment of MRF to the south of Nahavand, between $\sim 48.6^\circ$ and $\sim 48.8^\circ$ longitude. These epicenters define a narrow fault zone, about 3 km wide, that has a different trend from the seismicity discussed previously here, and in fact, a location and trend somewhat south of and more westerly-trending than the trace of the main Nahavand segment of the MRF. The two largest aftershocks (m_b 4.7 and 4.9) at 01:31 and 11:54 hrs, respectively, both occurred in this segment, the first of these occurring only 16 minutes after the mainshock. Thus, seismic activity began on the Nahavand segment immediately after the mainshock, but there is a gap of 10–12 km between the two patches (the solid black line in Fig. 4f), except for a small area of intense activity discussed next (item 3).
3. In the middle of the 10–12-km gap in seismic activity between the mainshock rupture zone and the activity on the Nahavand segment of the MRF, there is a small area of intense activity near the middle of the gap and at the northeastern edge of the Silakhour basin. Five events are located here (events 32, 35, 49, 52, and 56), effectively at the same location but over a span of a week. These are all small events, ranging in magnitude from m_b 2.1 to 2.7, but their concentration at a single location suggest that this may be the site of a small but significant barrier on the fault zone. This patch is also directly in line with the trend established by the western patch of seismicity discussed in item 2 of this section, separated from it by about 5 km.

Late Aftershocks

The later aftershocks (9 April–28 September) of the Silakhour sequence are shown in Figure 4e. Only two events in the cluster occurred after 30 April, an m_b 4.4 event on 17 June (event 79) in the Nahavand segment of the MRF and the last event on 28 September (event 80), which occurred in the aftershock zone of the mainshock (Dorud segment of the MRF). On the Nahavand segment, some of the late aftershocks (e.g., events 67, 73, and 75) are located a few kilometers away from the zone that was active immediately after the mainshock, perhaps indicating slow diffusion of stress away from the main rupture zone. Similarly, several of the late aftershocks (events 64, 65, and 70) on the Dorud segment of the MRF lie near or just beyond the edges of the mainshock rupture zone as defined by the early aftershocks. Alternatively, some of these events may be examples of outliers in the location procedure for which the true location lies

outside the confidence ellipse. Most of the late aftershocks on the Dorud segment appear to be associated with the northwestern end of the presumed rupture zone of the mainshock. Event 77 appears to be unrelated to the 2006 Silakhour sequence and perhaps should be associated with the background seismicity to the southwest of the MRF (Fig. 4a).

Discussion

A notable feature of our relocation analysis is that the 2006 Silakhour earthquake sequence is characterized by reactivation of two segments of the MRF, the Dorud segment to the southeast (representing the mainshock) and the Nahavand segment to the northwest. The two patches of seismicity are separated by about 10 km of the MRF, which remained nearly aseismic. We assert that the calibrated HDC analysis provides the highest resolution of the seismicity pattern in both relative and absolute terms, and our discussion will be based on the HDC locations presented in Table 2 and Figures 3 and 4.

Earthquake Location Bias

It is well understood that earthquake locations determined from phase arrival times can vary considerably, depending on the particular data set of arrival times that is used, the seismic velocity model from which theoretical times are calculated, and many technical aspects of the data processing, weighting, and inversion. For the 2006 Silakhour mainshock we list the hypocentral information from several standard catalogs in Table 4 and plot the epicenters on Figure 3. A few comments may be made:

- Most locations are biased to the southwest of the calibrated location by ~ 10 – 20 km. This is a result of irregular station coverage combined with imperfect travel-time models. The magnitude and direction of the bias is typical of similar studies conducted elsewhere in Iran (e.g., Walker *et al.*, 2005; Parsons *et al.*, 2006; Tatar *et al.*, 2007).
- The INSN epicenter is closest to the calibrated epicenter, about 5 km to the northwest. Although this network is relatively small, the network geometry (azimuthal coverage and station distances) for the Silakhour event was quite good. The other regional network in Iran (ITSN) contains more stations, but the azimuthal coverage for the Silakhour event was not as good. In other source regions, the location bias of the two regional networks could be quite different.
- Earthquake location bias in the Iran region could be reduced if the readings from the INSN and ITSN were routinely combined.

Relationship to the Main Recent Fault

The 2006 Silakhour mainshock epicenter is located at the southwestern edge of the pull-apart Silakhour basin, very close to the surface trace of the MRF (Fig. 3). The southwest edge of the basin is well known as an active fault zone

Table 4
Comparison of Hypocenters Determined by Various Agencies for the
Silakhour Mainshock

Number	Source*	Origin Time	Latitude (° N)	Longitude (° E)	Depth (km)
	HDC	0117:01.07	33.592	48.948	7.0
1	PDE	0117:00.96	33.50	48.78	7.0
2	EHB	0117:01.02	33.517	48.765	7.0
3	INSN	0117:02.3	33.65	48.91	14.0
4	ITSN	0117:04.3	33.483	48.864	18.0
5	EMSC	0116:59.3	33.50	48.73	9.0

*Sources: HDC, the epicenter determined by HDC analysis in this study (Table 2); PDE, the Preliminary Determination of Epicenters of the U.S. Geological Survey; EHB, the standard EHB catalog location (Engdahl *et al.*, 1998); INSN, the bulletin of the Iranian National Seismograph Network (operated by IIEES); ITSN, the bulletin of the Iranian Telemetered Seismograph Network (operated by the Institute of Geophysics, University of Tehran); EMSC, the bulletin of the European Mediterranean Seismological Center. The locations (other than HDC) are plotted on the map in Figure 3, labeled with the numbers in the first column.

(Tchalenko and Braud, 1974; Talebian and Jackson, 2002), but no surface rupture was observed for the 2006 mainshock to compare with the presumed trace of the fault based on field studies. Because the focal mechanism of the mainshock is strongly constrained to dip to the northeast at a relatively shallow angle, the fault plane, if continued to the surface, would emerge a few kilometers southwest of the trace of the MRF in shown in Figures 3 and 4. Peyret *et al.* (2008) suggest that the MRF dips northeast at depth, in accordance with the focal mechanism determined from several methods for the mainshock, but steepens at shallow depths where the crustal material is too weak to sustain coherent rupture. Our results are consistent with this view.

The aftershock activity directly associated with the mainshock rupture (Dorud patch) is mainly northeast (down-dip) of the mainshock epicenter, so the aftershocks' focal depths should in most cases be greater than that of the mainshock epicenter. Table 2 shows an increase of depth for the subset of events having reliable depth down-dip of the Dorud segment of the MRF. Because we are unable to resolve the depths for the majority of earthquakes in the Silakhour sequence at high accuracy, it could be that some of the aftershocks did occur at shallow depth (i.e., less than the 7 km depth at which they were fixed). If such events were associated with the mainshock rupture zone (Dorud patch), however, they would have occurred above the rupture plane of the mainshock (the hanging wall) because the relative locations constrain most of them to be northeast of the mainshock epicenter.

It is instructive to compare our conclusion about the location and dimensions of faulting in the mainshock with those of Peyret *et al.* (2008), who studied the slip distribution using InSAR and geodetic data. Their estimate (from a variable slip model) of a 15-km-long rupture zone, centered at ~5 km depth and extending approximately 6 km down-dip, is very consistent with our conclusions based on high-resolution locations of the mainshock and aftershocks. In the variable slip model, the maximum displacement is located

immediately under the village of Chalan-Chulan (Fig. 4f). Our location for the epicenter of the mainshock is located at the southeast edge of the zone of main rupture determined by Peyret *et al.* (2008).

We therefore conclude that our relocation of the Silakhour mainshock and the directly associated aftershocks (Dorud patch) are in close agreement with the location of faulting determined by Peyret *et al.* (2008). In particular, both studies show that the surface projection of the rupture zone lies northeast of the surface trace of the MRF, consistent with the occurrence of seismic activity at depth on a northeast-dipping fault. Because of the constraints on relative location provided by the HDC analysis, it follows that our locations of the second patch of aftershock activity, on the Nahavand trace of the MRF, as well as all other earthquakes in the cluster, are similarly bias free.

The Nahavand patch of aftershock activity forms a remarkably tight linear pattern only 2–3 km wide and about 20 km long, but it does not align closely with any major surface feature or the mapped trace of the MRF. It cuts across the right step of the MRF at the western end of the Silakhour basin with a trend similar to that of the very eastern end of the Nahavand–Borujerd segment of the MRF (Fig. 3), extending that trend across to the northeastern edge of the basin. The moment tensor solution of the largest aftershock in this patch (Fig. 3 and Table 3) has a steeper dip than those of the other events studied. A steeper dip of this fault segment could explain the narrowness of the associated pattern of epicenters. This pattern deviates rather significantly from the behavior that might be expected of an earthquake sequence on this section of the MRF, based on the topography and field mapping, indicating that the geometry of faulting in this area may be undergoing rapid evolution.

Unilateral Rupture

Our calibrated location for the epicenter of the mainshock is on the southeastern edge of the variable slip rupture zone

determined by [Peyret *et al.* \(2008\)](#), and aftershock activity is concentrated to the northwest. This geometry is consistent with largely unilateral rupture from southeast to northwest.

We can also investigate this feature of the rupture using the strong-motion recordings. Figure 5 shows the waveforms of the mainshock recorded at nearby strong-motion stations. We have compared the peak ground acceleration (PGA) of vertical component accelerograms, which are less sensitive than horizontal components, to site amplification ([Castro *et al.*, 1997](#)). The PGA at station Toos is much larger than that observed at stations Doro and Darr near Dorud (Fig. 5), even though the epicentral distances are similar. Using horizontal-to-vertical spectral ratios for the total *SH*-wave window, [Hamzehloo *et al.* \(2010\)](#) showed a significant amplification at strong-motion stations over the 2–5-Hz frequency band. We reproduced Figure 5 for both vertical and transverse components band-passed for the 2–5-Hz frequency band, finding that the PGA distribution for both band-passed vertical and transverse components still strongly favors a unidirectional rupture.

Further support for enhanced rupture propagation to the northwest was reported by [Mahdaviyar and Tajik \(2008\)](#), in a study of felt effects in the epicentral region. Isointensity contours are significantly asymmetric in the same manner as the distribution of PGA in Figure 5, elongated along strike of the MRF and extending further to the northwest than the southeast. These observations favor a rupture model that is mostly unilateral rupture oriented to the northwest.

Fault Dimensions

Aftershock locations have often been used to estimate the size of a mainshock rupture zone, but this relationship does not seem to hold in the case of the 2006 Silakhour sequence, for which the aftershocks extend between 50 and 60 km along strike. Surveys of rupture length of strike-slip earthquakes show that the expected length of an M_w 6.1 earthquake is normally in the range of 14 to 16 km (e.g., [Leonard, 2010](#); [Wells and Coppersmith, 1994](#)). We suggest that the solution to this inconsistency is to treat only a geographically restricted subset of the aftershocks, the so-called Dorud patch, as being directly related to the rupture of the mainshock.

Considering only the Dorud patch of aftershock activity, the inferred mainshock rupture zone has dimensions of ~15 km along strike and ~8 km across at the surface. An independent estimate for the fault length of the 2006 Silakhour mainshock comes from analysis of the InSAR data ([Peyret *et al.*, 2008](#)), which shows that rupture in the vicinity of Chalan-Chulan was confined to a zone 15–20 km in length that coincides with the Dorud patch of seismicity. Unfortunately, the interferogram coverage obtained by [Peyret *et al.* \(2008\)](#) did not include most of the Nahavand patch of seismicity, so we are lacking direct evidence of how much coseismic rupture, if any, occurred in that area. The seismic evidence is of two kinds, which are somewhat at odds:

1. The rupture area inferred from InSAR data, coinciding with the Dorud patch of seismicity, is very consistent with the observed magnitude of the event. If significant rupture occurred during the mainshock on the Nahavand segment of the MRF, the magnitude would be expected to be larger.
2. The source–time function (STF) for the mainshock ([Peyret *et al.*, 2008](#)) exhibits a secondary pulse of moment release, starting 2 s after the main pulse and lasting ~3 s. This secondary pulse could be interpreted as representing rupture to the northwest of the Dorud patch, either within the gap between the two seismicity patches (e.g., the locus of intense aftershock activity near 33.75° N, 48.90° E) or even on a portion of the MRF represented by the Nahavand patch of aftershocks.

We think the second argument is unlikely to be true for several reasons. The moment release of this second pulse is not large enough to be credibly associated with the rupture over the entire Nahavand patch. It is also possible that the secondary pulse of the STF is an artifact of the inversion, in which the STF parameters have absorbed the signal of crustal reverberations that are not adequately represented in the Green's function. Such observations are often made in body waveform inversion studies of shallow earthquakes and are frequently dismissed on these grounds. Furthermore, we have investigated the duration of rupture of the mainshock on the vertical component waveforms of the INSN broadband stations and measured it as 1.3–3.5 s in duration, depending on azimuth and distance of the recording station, with a mean of 2.6 s. There is no evidence of a significant secondary pulse of moment release. With the mean value of duration and a rupture velocity of 3.375 km/s ($0.9 V_S$), the fault length would be ~9 km for pure unilateral rupture ([Frankel and Kanamori, 1983](#)). Even with the maximum 3.5-s rupture duration, the inferred fault length is only ~12 km. If there is a component of bilateral rupture, as seems likely, the inferred rupture length would be greater and very consistent with the fault dimension inferred from aftershock locations in the Dorud patch and the variable slip model of [Peyret *et al.* \(2008\)](#).

Therefore, the aftershocks of the Nahavand patch, including the two largest aftershocks of the entire sequence, are unlikely to represent the mainshock's rupture area. We view these more distant events as perhaps triggered by stresses from the nearby rupture of the 2006 Silakhour mainshock (see [Stress Triggering](#)). The m_b 4.9 Borujerd event of 3 May 2005 and several other earlier events occurred in this patch, implying that this section of the MRF was already experiencing instability before the 2006 earthquake sequence.

Seismic Gap

The approximately 10-km-long gap in seismicity between the Dorud and Nahavand patches (Fig. 4f) corresponds (loosely) with a significant geometric deviation of the MRF and presumably represents a significant barrier to

through-going rupture. During the 2006 sequence, a series of small events occurred repeatedly at a specific site within the gap, but otherwise there is no evidence of slip having occurred in this region, from either the aftershock locations or the slip model of [Peyret et al. \(2008\)](#). If the gap were to be filled in a future earthquake, we would expect it to be of somewhat lesser magnitude than the 2006 Silakhour mainshock because the length of the potential rupture surface appears to be shorter.

The northwestern limit of rupture in the 23 January 1909 M_s 7.4 earthquake reported by [Ambraseys and Melville \(1982\)](#) abuts the rupture inferred for the 2006 Silakhour mainshock fairly closely (Fig. 3 and 4d), suggesting that there is little accumulated strain left in the intervening section of the MRF. As pointed out by [Peyret et al. \(2008\)](#), there is a continuing potential for rupture along the 50-km-long section of the MRF between the 2006 Silakhour event, perhaps including the Nahavand patch that was active in 2006, and the combined rupture zone of the 13 December 1957 Farsineh (M_w 6.8) and 16 August 1958 Nahavand (M_w 6.5) earthquakes (moment magnitudes from E. R. Engdahl, personal commun., 2010).

Stress Triggering

Triggering of off-plane near-field aftershocks has been frequently reported (e.g., [Das and Henry, 2003](#); [Gomberg et al., 2003](#); [Stacy et al., 2005](#)), most often in relation to strike-slip faulting and where there is significant unilateral rupture. “Near-field” is taken to mean a length scale of about one rupture length or less. We have discussed evidence that the Silakhour mainshock ruptured with a component of unilateral rupture toward the northwest, and our relocation study (Fig. 4d) clearly shows the existence of off-plane aftershock occurrence (the Nahavand patch) shortly after the mainshock, including the two largest aftershocks. [Gomberg et al. \(2003\)](#) present several similar examples. In the Silakhour cluster that was relocated by HDC, the first recorded aftershock is a large (m_b 4.7) event on the Nahavand patch ~16 minutes after the mainshock (event 19 in Table 2). To search for any smaller aftershocks that occurred between them, the continuous waveforms of all ITSN stations were reviewed. None were found. In addition to the two largest aftershocks, the Nahavand segment of the MRF experienced an m_b 4.9 event on 3 May 2005 (the Borujerd event), implying that it was already in an unstable state (unclamped). To examine if the aftershock cluster on the Nahavand segment can be attributed to the static stress change caused by the mainshock, we have calculated Coulomb stress change using dislocation calculations that simulate static earthquake slip in an elastic half-space ([Okada, 1992](#)). The Coulomb stress change, ΔCFS is

$$\Delta CFS = \Delta\tau + \mu(\Delta\sigma_n + \Delta P) = \Delta\tau + \mu'\Delta\sigma_n, \quad (1)$$

where $\Delta\tau$, $\Delta\sigma_n$, and ΔP are change in shear stress on a fault, change in normal stress, and change in pore pressure in the

fault zone, respectively. $\Delta\tau$ is positive for increasing shear stress in the direction of slip. $\Delta\sigma_n$ is positive for increasing tensional normal stress. The friction coefficient (μ) varies between 0 and 1. Usually ΔP has a tendency to counteract $\Delta\sigma_n$. Assuming that ΔP and μ do not depend on slip, the effect of ΔP can be considered by a reduced effective friction coefficient, μ' ([King et al., 1994](#)). Positive ΔCFS encourages failure and increase of aftershocks, and negative ΔCFS discourage failure.

Figure 7 shows the Coulomb stress-change field calculated at a depth of 8 km and the distribution of Silakhour seismic events. Superimposed on the figure is the location of the mainshock (white star) and aftershocks (circles) for the first 29 days after the mainshock. The Coulomb stress change is calculated for a nonuniform slip distribution, as calculated by the InSAR modeling of [Peyret et al. \(2008\)](#), on a fault dimension of 15 km length and 6 km along dip width. Following [Peyret et al. \(2008\)](#), a fault strike of 310° and a dip angle of 60° are used. The effective friction coefficient μ' is considered to be 0.4. Figure 7 clearly shows that aftershocks on the Nahavand segment, those to the southwest of the mainshock epicenter, and the majority of those concentrated along and in the northern part of the MRF lie within a region with Coulomb stress change greater than 0.1 bar. [Harris et al. \(1995\)](#) showed that regions with Coulomb stress change of larger than 0.1 bar are associated with earthquake triggering on neighboring faults. The pattern of the Coulomb stress-change field also fits the distribution of the aftershocks for a fault with dip angle of 45° , uniform slip fault with a 15 km length, and with down-dip width of 6 km. The ratio of discouraged versus encouraged aftershocks is not sensitive to μ' in the range of 0.4–0.8. From these observations, we conclude that the Nahavand patch of aftershock activity is a likely example of near-field static stress triggering.

Static stress triggering depends on the final distribution of slip, not on rupture directivity, and thus for an isotropic Earth model produces a symmetric stress distribution leading to a rather symmetric aftershock distribution ([Gomberg et al., 2003](#)), which is quite different from what is observed for the 2006 Silakhour sequence. Considering the relatively recent (1909) occurrence of a major earthquake southeast of the 2006 Silakhour event, an isotropic background stress field is probably unlikely in this case and may account for the asymmetry of off-plane aftershock activity.

The strong asymmetry of off-plane aftershocks does not need to be accounted for completely by stress changes related to the 2006 Silakhour mainshock. The 2005 m_b 4.9 Borujerd event and several others had already occurred on what would become the Nahavand patch (Fig. 4b).

Conclusions

We have studied the spatial distribution of seismicity associated with the 31 March 2006 Silakhour mainshock (M_w 6.1), using single- and multiple-event relocation, and with an unusually extensive data set of arrival time

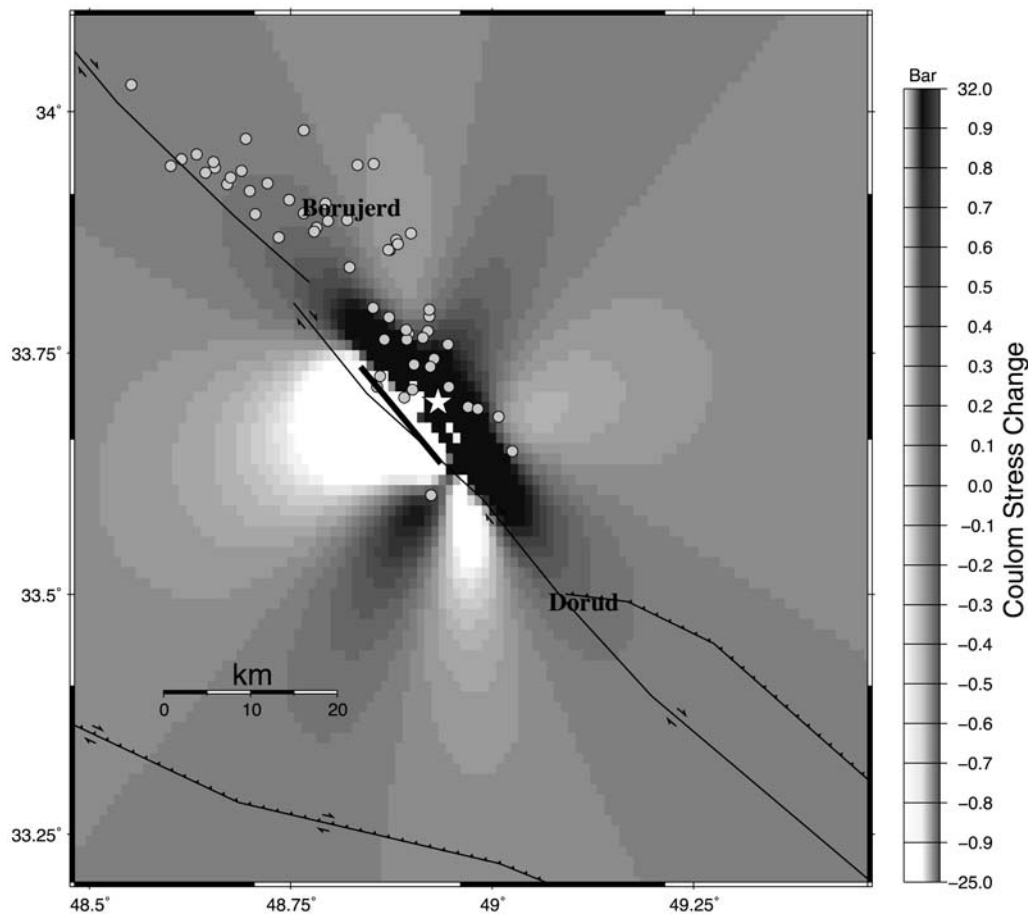


Figure 7. Static Coulomb stress change for the Silakhour main event calculated at a depth of 8 km. The white star shows the epicenter of the mainshock. The circles show the epicenter of the aftershocks for the first 29 days after the mainshock. The thick solid line shows the trace of the modeled fault, which has a strike of 310° and a slope of 60° toward the northeast. A nonuniform slip model of [Peyret *et al.* \(2008\)](#) is used.

information from permanent stations of several Iranian seismic networks, a temporary seismograph deployment, and a set of near-source accelerometers, supplemented by phase arrival readings from many stations outside Iran at regional to teleseismic distances. We have also studied the source mechanisms of the mainshock and three other events with a regional moment tensor analysis. Our moment tensor inversion shows a mostly right-lateral strike-slip faulting with strike favorably parallel to the MRF for the mainshock, the two large foreshocks, and the larger aftershock event.

The details of the seismicity pattern are revealed most clearly in a multiple-event relocation study that is specialized to determine bias-free (calibrated) absolute locations. The accuracy of these locations is confirmed by comparison of the seismicity pattern with a slip model of the mainshock from InSAR data ([Peyret *et al.*, 2008](#)). The seismicity pattern lies along the southern edge of the Silakhour basin, where most investigators have placed the active trace of the MRF. The epicenters of aftershocks generally lie to the northeast of the mainshock epicenter, consistent with focal mechanism analyses of the mainshock that reveal right-lateral strike-slip motion on a northeast-dipping fault subparallel to the MRF,

and with most aftershocks occurring down-dip of the shallow mainshock rupture zone.

The 50–60-km-long overall pattern of seismicity is divided primarily into two discrete patches that are associated with two segments of the MRF: a 20–25-km patch of seismicity on the Nahavand segment of the MRF and a 15–20-km patch of seismicity associated with the Dorud segment of the MRF. The Nahavand patch is offset to the northeast by ~ 5 km relative to the Dorud patch, broadly reflecting the discontinuity of the mapped MRF segments. Only the Dorud patch is directly associated with the mainshock rupture. Both the Nahavand and Dorud patches were seismically active at low levels in recent decades. The location and orientation of the Nahavand patch of seismicity bears only a loose resemblance to the surface geology of the MRF between Borujerd and Nahavand. We take this as evidence of ongoing evolution of the geometry of faulting along this portion of the MRF.

Based on the location of the mainshock epicenter relative to aftershocks and the variable-slip rupture model based on InSAR analysis ([Peyret *et al.*, 2008](#)), and also from the distribution of PGA, the mainshock rupture initiated near the

southeastern end of the rupture zone and propagated predominantly unilaterally toward the northwest. Between the two patches of seismicity is a gap of ~ 10 km, except for a very localized site of persistent low-magnitude aftershock activity. This gap appears to represent a section of the MRF that did not fail in the 2006 sequence and could be capable of generating an earthquake in the magnitude range 5.5–6.0 in the future.

Coseismic rupture in the 31 March mainshock was confined to the Dorud patch, but the Nahavand patch experienced the largest aftershocks and approximately half of all the recorded aftershocks, beginning no more than 16 minutes after the mainshock. The Nahavand patch was likely triggered by static stress changes related to the mainshock rupture.

Data and Resources

The geological provinces in Figure 1 are modified from the structural map of the National Geoscience Database of Iran (NGDIR; <http://www.ngdir.ir>). The events of the Silakhour sequence were located with a standard single-event approach, the program HYPOCENTRE (Lienert and Havskov, 1995), from the SEISAN software package (Havskov and Otemoller, 1999).

Phase arrival time data, waveform data, and information about the networks whose data were used in this study can be accessed at the following websites:

- Iran Seismic Centre (IRSC): <http://irsc.ut.ac.ir> (last accessed July 2011).
- International Institute of Earthquake Engineering and Seismology (IIIES): <http://www.iiies.ac.ir> (last accessed July 2011).
- Building and Housing Research Center (BHRC): <http://bhrc.ac.ir> (last accessed July 2011).
- International Seismological Centre (ISC): <http://www.isc.ac.uk> (last accessed July 2011).
- International Seismological Summary (ISS): http://earthquake.usgs.gov/research/data/iss_summ.php (last accessed July 2011).
- National Earthquake Information Center (NEIC): <http://neic.usgs.gov> (last accessed July 2011).
- Global CMT: <http://www.globalcmt.org> (last accessed July 2011).

Acknowledgments

The authors thank the Institute of Geophysics, University of Tehran, International Institute of Earthquake Engineering and Seismology, and the Building and Housing Research Center for providing us with data. We are very grateful to F. Yamini-Fard for providing data from the temporary network deployment. We thank N. Kamalian for his efforts in providing us the seismic records from the Kharkeh Dam network. We greatly appreciate Dirk Roessler from the University of Potsdam, Germany, for allowing us to use his scripts to produce Figure 6.

References

- Ambraseys, N. N., and C. P. Melville (1982). *A History of Persian Earthquakes*, Cambridge University Press, Cambridge, United Kingdom, 240 pp.
- Ambraseys, N. N., and A. Moinfar (1973). The seismicity of Iran: The Silakhor (Lurestan) earthquake of 23rd January 1909, *Ann. Geophys.* **26**, 659–678.
- Biggs, J., E. Bergman, B. Emmerson, G. Funning, J. Jackson, B. Parsons, and T. Wright (2006). Fault identification for buried strike-slip earthquakes using InSAR: The 1994 and 2004 Al Hoceima, Morocco earthquakes, *Geophys. J. Int.* **166**, 1347–1362.
- Bondar, I., E. A. Bergman, E. R. Engdahl, B. Kohl, Y.-L. Kung, and K. McLaughlin (2008). A hybrid multiple event location technique to obtain ground truth event locations, *Geophys. J. Int.* **175**, 185–201.
- Bondar, I., S. C. Myers, E. R. Engdahl, and E. A. Bergman (2004). Epicentre accuracy based on seismic network criteria, *Geophys. J. Int.* **156**, 483–496.
- Castro, R. R., M. Mucciarelli, F. Pacor, and C. Petrongaro (1997). S-wave site-response estimates using horizontal-to-vertical spectral ratios, *Bull. Seismol. Soc. Am.* **87**, 256–260.
- Chu, D., and R. G. Gordon (1998). Current plate motions across the Red Sea, *Geophys. J. Int.* **135**, 313–328.
- Croux, C., and P. J. Rousseeuw (1992). Time-efficient algorithms for two highly robust estimators of scale, *Comput. Stat.* **1**, 411–428.
- Dahm, T., F. Krüger, K. Stammer, K. Kinge, R. Kind, K. Wylegalla, and J. R. Grasso (2007). The 2004 M_w 4.4 Rotenburg, northern Germany, earthquake and its possible relationship with gas recovery, *Bull. Seismol. Soc. Amer.* **97**, 691–704.
- Dahm, T., G. Manthei, and J. Eisenblätter (1999). Automated moment tensor inversion to estimate source mechanisms of hydraulically induced micro-seismicity in salt rock, *Tectonophysics* **306**, 1–17.
- Das, S., and C. Henry (2003). Spatial relation between main earthquake slip and its aftershock distribution, *Rev. Geophys.* **41**, 1013, doi [10.1029/2002RG000119](https://doi.org/10.1029/2002RG000119).
- De Mets, C., R. G. Gordon, D. F. Argus, and S. Stein (1994). Effect of recent revision to the geomagnetic reversal time scale on the estimates of current plate motions, *Geophys. Res. Lett.* **21**, 2191–2194.
- Doloei, J., and R. Roberts (2003). Crustal and uppermost mantle structure of Tehran region from teleseismic P-waveform receiver function analysis, *Tectonophysics* **364**, 115–133.
- Engdahl, E. R., R. van der Hilst, and R. Buland (1998). Global teleseismic earthquake relocation with improved travel times and procedures for depth determination, *Bull. Seismol. Soc. Am.* **88**, 722–743.
- Frankel, A., and H. Kanamori (1983). Determination of rupture duration and stress drop for earthquakes in southern California, *Bull. Seismol. Soc. Am.* **73**, 1527–1551.
- Ghods, A., and F. Sobouti (2005). Quality assessment of seismic recording: Tehran Seismic Telemetry Network, *Asian J. Earth Sci.* **25**, 687–694.
- Gomberg, J., P. Bodin, and P. A. Reasenberg (2003). Observing earthquakes triggered in the near field by dynamic deformations, *Bull. Seismol. Soc. Am.* **93**, 118–138.
- Hamzehloo, H., H. Rahimi, I. Sarkar, M. Mahood, H. Mirzaei Alavijeh, and E. Farzanegan (2010). Modeling the strong ground motion and rupture characteristics of the March 31, 2006, Darb-e-Astane earthquake, Iran, using a hybrid of near-field SH-wave and empirical Green's function method, *J. Seismol.* **14**, doi [10.1007/s10950-009-9159-x](https://doi.org/10.1007/s10950-009-9159-x).
- Harris, R. A., R. W. Simpson, and P. A. Reasenberg (1995). Influence of static stress changes on earthquake locations in southern California, *Nature* **375**, 221–224.
- Havskov, J., and L. Otemoller (1999). SEISAN: The Earthquake Analysis Software, version 8.0, Institute of Solid Earth Physics, University of Bergen, Norway.
- Hessami, K., F. Jamali, and H. Tabassi (2003). Major Active Faults of Iran (map), scale 1:2,500,000. Ministry of Science, Research and Technology, International Institute of Earthquake Engineering and Seismology.

- Hutton, L. K., and D. M. Boore (1987). The M_L scale in southern California, *Bull. Seismol. Soc. Amer.* **77**, 2074–2094.
- Jackson, J. (1992). Partitioning of strike-slip and convergent motion between Eurasia and Arabia in eastern Turkey and the Caucasus, *J. Geophys. Res.* **97**, 12,471–12,479.
- Jordan, T. H., and K. A. Sverdrup (1981). Teleseismic location techniques and their application to earthquake clusters in the south-central Pacific, *Bull. Seismol. Soc. Am.* **71**, 1105–1130.
- Kaviani, A. (2004). La chaîne de collision continentale du Zagros (Iran): Structure lithosphérique par analyse de données sismologiques, *Ph.D. Thesis*, University of Joseph Fourier-Grenoble I.
- King, G. C. P., R. S. Stein, and J. Lin (1995). Static stress changes and the triggering of earthquakes, *Bull. Seismol. Soc. Am.* **84**, 935–953.
- Leonard, M. (2010). Earthquake fault scaling: Self-consistent relating of rupture length, width, average displacement, and moment release, *Bull. Seismol. Soc. Am.* **100**, 1971–1988.
- Lienert, B. R., and J. Havskov (1995). A computer program for locating earthquakes both locally and globally, *Seismol. Res. Lett.* **66**, 26–36.
- Ma, S., and G. M. Atkinson (2006). Focal depths for small to moderate earthquakes ($m_n \geq 2.8$) in western Quebec, southern Ontario, and northern New York, *Bull. Seismol. Soc. Am.* **96**, 609–623.
- Mahdaviifar, M., and V. Tajik (2008). Geotechnical aspects of Darbe Astaneh earthquake (March 31, 2006, Borujerd, Iran), <http://www.ies.ac.ir/bank/Broujerd/fasl-3.pdf>. (last accessed June 2010; in Farsi).
- Mirzaie Alevijeh, H., E. Farzanegan, M. H. Majedi Ardekani, and F. Sinaeian (2006). Silakhor earthquake March 31 2006, Building and Housing Research Center, Tehran, Iran, 54 pp. (in Farsi).
- Muller, G. (1985). The reflectivity method: A tutorial, *J. Geophys.* **58**, 153–174.
- Okada, Y. (1992). Internal deformation due to shear and tensile faults in a half-space, *Bull. Seismol. Soc. Am.* **82**, 1018–1040.
- Parsons, B., T. Wright, P. Rowe, J. Andrews, J. Jackson, R. Walker, M. Khatib, M. Talebian, E. Bergman, and E. R. Engdahl (2006). The 1994 Sefidabeh (eastern Iran) earthquakes revisited: New evidence from satellite radar interferometry and carbonate dating about the growth of an active fold above a blind thrust fault, *Geophys. J. Int.* **164**, 202–217.
- Peyret, M., F. Rolandone, S. Dominguez, Y. Djamour, and B. Meyer (2008). Source model for the M_w 6.1, 31 March 2006, Chalan-Chulan earthquake (Iran) from InSAR, *Terra Nova* **20**, 126–133.
- Stacy, S., J. Gomberg, and M. Cocco (2005). Introduction to special section: Stress transfer, earthquake triggering, and time-dependent seismic hazard, *J. Geophys. Res.* **110**, no. B05S01, doi [10.1029/2005JB003692](https://doi.org/10.1029/2005JB003692).
- Talebian, M., and J. Jackson (2002). Offset on the Main Recent Fault of NW Iran and implications for the late Cenozoic tectonics of the Arabia—Eurasia collision zone, *Geophys. J. Int.* **150**, 422–439.
- Tatar, M. (2001). Etude sismotectonique de deux zones de collision continentale: Le Zagros Central et l'Alborz (Iran), *Ph.D. Thesis*, University of Joseph Fourier-Grenoble I.
- Tatar, M., J. Jackson, D. Hatzfeld, and E. A. Bergman (2007). The 28 May 2004 Baladeh earthquake (M_w 6.2) in the Alborz, Iran: Implications for the geology of the south Caspian basin margin and for the seismic hazard of Tehran, *Geophys. J. Int.* **170**, 249–261.
- Tchalenko, J. S., and J. Braud (1974). Seismicity and structure of the Zagros: The Main Recent Fault between 33° and 55° N, *Phil. Trans. Roy. Soc. Lond. A* **277**, 1–25.
- Walker, R. T., E. Bergman, J. Jackson, M. Ghorashi, and M. Talebian (2005). The 2002 June 22 Changureh (Avaj) earthquake in Qazvin Province, northwest Iran: Epicentral relocation, source parameters, surface deformation and geomorphology, *Geophys. J. Int.* **160**, 707–720.
- Wells, D. L., and K. J. Coppersmith (1994). New empirical relationships among magnitude, rupture length, rupture width, rupture area, and surface displacement, *Bull. Seismol. Soc. Am.* **84**, 974–1002.

Department of Earth Sciences
Institute for Advanced Studies in Basic Sciences
Gava Zang, P.O. Box 45195-159
Zanjan, Iran
aghods@iasbs.ac.ir
(A.G., G.M.)

Institute of Geophysics
University of Tehran
Post Box 14155-6466
Tehran 1435944411
Iran
rezapour@ut.ac.ir
(M.R.)

Center for Imaging the Earth's Interior
Department of Physics
University of Colorado
Boulder, Colorado 80309-0390
Eric.Bergman@Colorado.EDU
(E.B.)

Research Institute for Earth Sciences
Geological Survey of Iran
Post Box 13185-1494
Azadi Sq., Meraj-street
Tehran, Iran
Talebian@gsi.ir
(M.T.)

Manuscript received 7 January 2011